ECCOMAS Congress 2016
VII European Congress on Computational Methods in Applied Sciences and Engineering
M. Papadrakakis, V. Papadopoulos, G. Stefanou, V. Plevris (eds.)
Crete Island, Greece, 5–10 June 2016

A THERMODYNAMICALLY CONSISTENT FINITE STRAIN MICRO-SPHERE FRAMEWORK FOR PHASE-TRANSFORMATIONS

R. Ostwald[1], **T. Bartel**[1], **and A. Menzel**[1,2]

[1]Institute of Mechanics, TU Dortmund University
Leonhard-Euler-Str. 5, D-44227 Dortmund, Germany
e-mail: richard.ostwald@udo.edu / thorsten.bartel@udo.edu / andreas.menzel@udo.edu

[2] Division of Solid Mechanics, Lund University
P.O. Box 118, SE-22100 Lund, Sweden
e-mail: andreas.menzel@solid.lth.se

Keywords: Finite strain, Micro-sphere, Phase-transformation

Abstract. *We extend a thermodynamically consistent finite strain micro-sphere framework elaborated by Carol et al. towards the modelling of phase-transformations to allow for the simulation of polycrystalline solids such as, e.g., shape memory alloys and shape memory polymers undergoing large deformations. The considered phase-transformation mechanism is based on statistical physics and allows the consideration of an arbitrary number of solid material phases. The specifically constructed, non-quadratic Helmholtz free energy functions considered in every micro-plane of the micro-sphere framework are extended to include individual Bain-type transformation strains for each of the phases. The total strains acting in each material phase are multiplicatively decomposed into elastic strains and transformation strains.*

1 INTRODUCTION

The physical mechanisms and effects accompanied by phase-transformations in solids present a large potential for industrial applications. For example, NiTi-based shape memory alloys (SMA) are used in medical applications [1], aerospace technology [2] and other industrial fields, cf., e.g., [3, 4].

During tensile deformation of such material—after exceeding the purely elastic regime of the, e.g. austenitic, parent phase—the onset of phase-transformations is accompanied by a plateau-type stress-strain relation, finally followed by a sharp rise in the specimen stress. The latter indicates the completion of the transformation process, resulting again in an elastic behaviour of the now completely transformed material. Considering a polycrystalline material at the meso-scale, however, it is important to note that an initially purely austenitic crystal will not transform to $100\,\%$ martensite. Unfavourably oriented grains within the polycrystalline arrangement might not transform at all—furthermore, experimental observations suggest that even favourably oriented grains usually only transform to a certain extent as elaborated in, e.g., [5].

This so-called grain locking effect within a crystal is related to the sequential transformation behaviour of individual grains. In other words, the initial onset of transformation in the most favourably oriented grain is accompanied by a change of the elastic stress state in its surrounding area, i.e. in its neighboured grains. This change of stress state can hinder transformation in a neighboured grain, especially if a formerly favourable stress state within a particular neighbouring grain turns into an unfavourable stress state.

Taking into account complex interactions at the micro-scale—such as specific microstructure arrangements and twin formations—leads to reliable micromechanical material models, such as the ones presented in, e.g., [6, 7, 8, 9, 10, 11, 12, 13, 14]. However, a possible disadvantage of such precise modelling approaches might be the high computational costs that usually accompany the detailed capturing of microstructural material effects. On the other hand, purely phenomenological models facilitate the solution of complex macroscopic initial boundary value problems (IBVPs) via finite element simulations. Typical phenomenological approaches such as the ones presented in [15, 16, 17], are usually derived within thermodynamical frameworks. Besides the application of the first and second law of thermodynamics, generalised irreversible forces and fluxes, cf. [18] amongst others, are considered in view of a consistent derivation of evolution equations for the inelastic constitutive variables. For the application of phenomenological models in view of efficient macro-scale simulations, the underlying specific modelling parameters need to be fitted to experimentally observed material behaviour for different, representative loading paths [19, 20, 21]. Such phase-transformation models are usually based on classic plasticity-type approaches regarding the onset of the transformation process. While early models were formulated in a one-dimensional setting with restriction to states of tensile stress [22], more sophisticated frameworks are established in, e.g., [16, 15, 23]. Constitutive frameworks that focus on the simulation of single crystals are provided in [24, 25, 26] amongst others.

Another class of thermodynamical models makes use of statistical considerations, capturing transformation probabilities that are derived based on statistical physics. In this context, energy barriers related to the Gibbs potentials of the individual phases need to be determined for the computation of the desired transformation probabilities [27, 28]. Such models have recently been implemented in small strain affine and non-affine micro-sphere frameworks, [29, 30] and [31, 32], respectively. The goal of this contribution is to provide an ansatz for a finite

strain micro-sphere phase-transformation model based on statistical physics, where we use a thermodynamically consistent microsphere framework established in [33] as a basis. For the sake of conceptual clarity, we restrict the subsequent formulation to two phases—one austenitic parent phase and a single martensite variant.

2 MICRO-PLANE CONSTITUTIVE FORMULATION

This section presents a finite strain generalisation of previous phase-transformation models by the authors, cf. [29, 30]. To this end, we consider a finite strain micro-plane constitutive formulation for Neo-Hookean-type elasticity introduced in [33] as a basis, which is extended towards phase-transformations. The micro-plane constitutive relation for phase-transformations is then embedded into a corresponding micro-sphere framework in view of the solution of three-dimensional initial boundary value problems.

2.1 DEFINITION OF VOLUME FRACTIONS

The volume fraction ξ_N^α associated to a particular phase $\alpha \in \{\mathrm{A}, \mathrm{M}\}$, where A represents austenite and M represents martensite, associated to the micro-plane with orientation N is defined as

$$\xi_N^\alpha := \lim_{v_N \to 0} \left(\frac{v_N^\alpha}{v_N} \right) \tag{1}$$

and must at any time obey the restrictions

$$\xi_N^\alpha \in \ [0,1] \subset \mathbb{R} \quad , \quad \sum_\alpha \xi_N^\alpha = \ 1 \quad , \quad \sum_\alpha \dot{\xi}_N^\alpha = \ 0 \quad , \tag{2}$$

as both the austenite and the martensite phase are assumed to possess identical time-independent referential mass densities $\rho^\alpha = \rho_0 = \mathrm{const}$.

2.2 MICRO-PLANE STRAIN MEASURE

Generally speaking, different micro-plane strain measures can be considered within a micro-sphere framework. However, in view of capturing a macroscopic Neo-Hookean type material response for the individual phases—and in line with [33]—we restrict the formulation to a certain normal strain measure. Specifically, we characterise the normal strain acting on the micro-plane as

$$\lambda_N = ||\boldsymbol{F} \cdot \boldsymbol{N}|| = \sqrt{\boldsymbol{N} \cdot \boldsymbol{C} \cdot \boldsymbol{N}} \tag{3}$$

with $\boldsymbol{F}$ representing the deformation gradient and $\boldsymbol{C} = \boldsymbol{F}^{\mathrm{t}} \cdot \boldsymbol{F}$ being the right Cauchy-Green deformation tensor. Note that the restriction to this strain measure induces a macroscopic Poisson's ratio of $\nu_{\mathrm{P}} = 0.25$.

2.3 MULTIPLICATIVE MICRO-STRAIN DECOMPOSITION

For the consideration of Bain-type transformation strains associated to the martensite phase, the total micro-plane strain measure (3) is multiplicatively decomposed into an elastic strain contribution λ_N^α and a transformation related contribution $\lambda_{\mathrm{tr}}^\alpha$ via

$$\lambda_N = \lambda_N^\alpha \, \lambda_{\mathrm{tr}}^\alpha \, , \tag{4}$$

so that the elastic strain contribution λ_N^α that enters the free energy potentials of the respective material phase α takes the form

$$\lambda_N^\alpha = \lambda_N \, [\lambda_{\mathrm{tr}}^\alpha]^{-1} \tag{5}$$

with the total strain measure λ_N defined in (3) and with an individual material constant $\lambda_{\rm tr}^{\alpha}$ for both austenite and martensite.

2.4 MICRO-PLANE HELMHOLTZ FREE ENERGY POTENTIALS

For each phase α situated within a micro-plane with orientation N we consider a micro-plane Helmholtz free energy $\psi_N^{\alpha} = \widehat{\psi}_N^{\alpha}(\lambda_N)$ of the form

$$\widehat{\psi}_N^{\alpha}(\lambda_N) = \mathsf{E}^{\alpha} \left[\frac{\left[\lambda_N \left[\lambda_{\rm tr}^{\alpha}\right]^{-1}\right]^2}{2} + \frac{\left[\lambda_N \left[\lambda_{\rm tr}^{\alpha}\right]^{-1}\right]^{-3}}{3} - \frac{5}{6} \right] , \tag{6}$$

with E^{α} denoting the scalar-valued micro-plane elasticity coefficent of phase α, $\lambda_{\rm tr}^{\alpha}$ being the corresponding transformation strain, and λ_N representing the micro-plane strain measure defined in (3). Note that this format of the Helmholtz free energy represents a natural extension of the energy term proposed in [33] towards the consideration of transformation strains $\lambda_{\rm tr}^{\alpha}$ within the individual phases α. For the transformation strain in the austenitic parent phase we have $\lambda_{\rm tr}^{\rm A} = [\lambda_{\rm tr}^{\rm A}]^{-1} = 1$, thus for austenite the Helmholtz free energy potential (6) simplifies to

$$\widehat{\psi}_N^{\rm A}(\lambda_N) = \mathsf{E}^{\rm A} \left[\frac{\lambda_N^2}{2} + \frac{\lambda_N^{-3}}{3} - \frac{5}{6} \right] , \tag{7}$$

which is directly related to the format proposed in [33] for the compressible extension of a micro-sphere model with vanishing initial microstresses.

Accordingly, the material micro-plane stress $S_N^{\alpha} = \widehat{S}^{\alpha}(\lambda_N)$ corresponding to each phase α takes the form

$$\widehat{S}_N^{\alpha}(\lambda_N) = \frac{\partial \widehat{\psi}_N^{\alpha}(\lambda_N)}{\partial \lambda_N} \tag{8}$$

$$= \mathsf{E}^{\alpha} \, [\lambda_{\rm tr}^{\alpha}]^{-1} \left[\left[\lambda_N \left[\lambda_{\rm tr}^{\alpha}\right]^{-1}\right] - \left[\lambda_N \left[\lambda_{\rm tr}^{\alpha}\right]^{-1}\right]^{-4} \right] . \tag{9}$$

The overall Helmholtz free energy $\Psi_N = \widehat{\Psi}_N(\lambda_N)$ of the considered multi-phase mixture associated to the micro-plane with spatial orientation N is obtained from the contributions of the respective constituents, i.e.

$$\widehat{\Psi}_N(\lambda_N) = \sum_{\alpha} \xi_N^{\alpha} \, \widehat{\psi}_N^{\alpha}(\lambda_N) \tag{10}$$

$$= \sum_{\alpha} \xi_N^{\alpha} \, \mathsf{E}^{\alpha} \left[\frac{\left[\lambda_N \left[\lambda_{\rm tr}^{\alpha}\right]^{-1}\right]^2}{2} + \frac{\left[\lambda_N \left[\lambda_{\rm tr}^{\alpha}\right]^{-1}\right]^{-3}}{3} - \frac{5}{6} \right] , \tag{11}$$

where ξ_N^{α} is the volume fraction of phase α as defined in (1). The resulting overall material micro-plane stress measure $S_N = \widehat{S}_N(\lambda_N)$ of the mixture follows from the combination of (8)

and (10), namely

$$\widehat{S}_N(\lambda_N) = \frac{\partial \widehat{\Psi}_N(\lambda_N)}{\partial \lambda_N} \tag{12}$$

$$= \frac{\partial}{\partial \lambda_N}\left[\sum_\alpha \xi_N^\alpha\, \widehat{\psi}_N^\alpha(\lambda_N)\right] \tag{13}$$

$$= \sum_\alpha \frac{\partial}{\partial \lambda_N}\left[\xi_N^\alpha\, \widehat{\psi}_N^\alpha(\lambda_N)\right] \tag{14}$$

$$= \sum_\alpha \xi_N^\alpha\, \frac{\partial \widehat{\psi}_N^\alpha(\lambda_N)}{\partial \lambda_N} \tag{15}$$

$$= \sum_\alpha \xi_N^\alpha\, \widehat{S}_N^\alpha(\lambda_N) \tag{16}$$

$$= \sum_\alpha \xi_N^\alpha\, \mathsf{E}^\alpha\, [\lambda_{\mathrm{tr}}^\alpha]^{-1}\left[\left[\lambda_N\,[\lambda_{\mathrm{tr}}^\alpha]^{-1}\right] - \left[\lambda_N\,[\lambda_{\mathrm{tr}}^\alpha]^{-1}\right]^{-4}\right] . \tag{17}$$

2.5 MICRO-PLANE GIBBS FREE ENERGY POTENTIALS

The individual micro-plane Helmholtz free energy potentials ψ_N specified in Section 2.4, cf. (6), are transformed to a Gibbs potential $g_N^\alpha = \widehat{g}_N^\alpha(\lambda_N^*)$ using a Legendre transformation. Note that λ_N^* corresponds to a parametrisation of the micro-plane strain space, whereas λ_N reflects the actual, physical micro-plane strain that the considered material mixture is subjected to. With the considered micro-plane strain measure λ_N as the functional variable of the Helmholtz free energy of phase α, the Legendre transformation of the latter energy is accomplished by means of

$$\widehat{g}_N^\alpha(\lambda_N^*) = \widehat{\psi}_N^\alpha(\lambda_N^*) - \lambda_N^*\, \frac{\partial \widehat{\psi}^\alpha(\lambda_N)}{\partial \lambda_N}\bigg|_{\lambda_N} \tag{18}$$

$$= \widehat{\psi}_N^\alpha(\lambda_N^*) - \lambda_N^*\, \widehat{S}_N^\alpha(\lambda_N)\Big|_{\lambda_N} \tag{19}$$

$$= \widehat{\psi}_N^\alpha(\lambda_N^*) - \lambda_N^*\, S_N^\alpha\,, \tag{20}$$

where use has been made of (8). Note that the partial derivative in (18) reflects the material stress contribution corresponding to phase α of the mixture, the evaluation of which according to (9) for the current stretch state λ_N yields the specific stress contribution S_N^α of phase α present in the considered micro-plane.

For the evolution of volume fractions provided in Section 2.6, the Gibbs potential (25) that is parameterised in terms of a fictitious stretch λ_N^* takes the specific form

$$\widehat{g}_N^\alpha(\lambda_N^*) = \widehat{\psi}_N^\alpha(\lambda_N^*) - \lambda_N^*\, S_N^\alpha \tag{21}$$

$$= \mathsf{E}^\alpha\left[\frac{\left[\lambda_N^*\,[\lambda_{\mathrm{tr}}^\alpha]^{-1}\right]^2}{2} + \frac{\left[\lambda_N^*\,[\lambda_{\mathrm{tr}}^\alpha]^{-1}\right]^{-3}}{3} - \frac{5}{6}\right] - \lambda_N^*\, S_N^\alpha \tag{22}$$

where use has been made of (6).

In a similar fashion, the overall micro-plane Helmholtz free energy potential Ψ_N of the mixture specified in Section 2.4 is transformed to an overall Gibbs potential $G_N = \widehat{G}_N(\lambda_N^*)$ using

a Legendre transformation, specifically

$$\widehat{G}_N(\lambda_N^*) = \widehat{\Psi}_N(\lambda_N^*) - \lambda_N^* \left. \frac{\partial \widehat{\Psi}_N(\lambda_N)}{\partial \lambda_N} \right|_{\lambda_N} \tag{23}$$

$$= \widehat{\Psi}_N(\lambda_N^*) - \lambda_N^* \left. \widehat{S}_N(\lambda_N) \right|_{\lambda_N} \tag{24}$$

$$= \widehat{\Psi}_N(\lambda_N^*) - \lambda_N^* S_N \, . \tag{25}$$

Note that the partial derivative in (23) reflects the material stress currently acting within the mixture due to the externally applied material stretch λ_N, the evaluation of which according to (17) for the current stretch state λ_N yields the overall stress value S_N acting on the micro-plane under consideration.

The combination of (23) with (10) and (15) yields

$$\widehat{G}_N(\lambda_N^*) = \sum_\alpha \xi_N^\alpha \, \widehat{\psi}_N^\alpha(\lambda_N^*) - \lambda_N^* \left[\sum_\alpha \xi_N^\alpha \left. \frac{\partial \widehat{\psi}_N^\alpha(\lambda_N)}{\partial \lambda_N} \right|_{\lambda_N} \right] \tag{26}$$

$$= \sum_\alpha \xi_N^\alpha \left[\widehat{\psi}_N^\alpha(\lambda_N^*) - \lambda_N^* \left. \widehat{S}_N^\alpha(\lambda_N) \right|_{\lambda_N} \right] \tag{27}$$

$$= \sum_\alpha \xi_N^\alpha \, \widehat{g}_N^\alpha(\lambda_N^*) \, , \tag{28}$$

i.e. the overall Gibbs potential $\widehat{G}_N(\lambda_N^*)$ is obtained from the contributions of the individual constituents, which is consistent to the relation obtained for the overall Helmholtz free energy potential, cf. (10).

2.6 EVOLUTION OF VOLUME FRACTIONS

The approach used for the derivation of the differential equations governing the evolution of volume fractions is based on statistical physics, cf. [27]. In this context, a transformation probability matrix $\boldsymbol{Q} = \widehat{\boldsymbol{Q}}(\boldsymbol{\xi}) \in \mathbb{R}^{2\times 2}$ corresponding to an infinitesimal generator of a Markov process is introduced, see also [28]. The transformation probability matrix drives the evolution of volume fractions via

$$\dot{\boldsymbol{\xi}} = \widehat{\boldsymbol{Q}}(\boldsymbol{\xi}) \cdot \boldsymbol{\xi} \, , \tag{29}$$

wherein the notation $\dot{\bullet}$ denotes the material time derivative. For the two-phase transformation between austenite A and martensite M considered in the contribution at hand, the transformation probability matrix takes the form

$$\boldsymbol{Q} = \omega \begin{bmatrix} -P_{\mathrm{A}\to\mathrm{M}} & P_{\mathrm{M}\to\mathrm{A}} \\ P_{\mathrm{A}\to\mathrm{M}} & -P_{\mathrm{M}\to\mathrm{A}} \end{bmatrix} \neq \boldsymbol{Q}^{\mathrm{t}} \tag{30}$$

with ω being a material parameter denoted as transition attempt frequency and

$$P_{\mathrm{A}\to\mathrm{M}} = \widehat{P}_{\mathrm{A}\to\mathrm{M}}(b_{\mathrm{A}\to\mathrm{M}}) \in [0,1] \subset \mathbb{R} \tag{31}$$

as well as

$$P_{\mathrm{M}\to\mathrm{A}} = \widehat{P}_{\mathrm{M}\to\mathrm{A}}(b_{\mathrm{M}\to\mathrm{A}}) \in [0,1] \subset \mathbb{R} \tag{32}$$

representing the probability for the transformation of austenite A to martensite M and vice versa, respectively. Note that the sum of elements in each column of $\boldsymbol{Q}$ is zero, i.e. $\sum_i Q_{ij} = 0 \; \forall \; j$ holds, inducing a so-called conservative Markov process. It can be shown that this special structure of the system of evolution equations ensures that the physical restrictions (2) regarding the volume fractions ξ^{A} and ξ^{M} are fulfilled without the need to enforce any additional algebraic inequality constraints on the system of evolution equations, cf. also [27].

In particular, according to [27], the probability for the transformation from one phase α into another phase β follows from

$$P_{\alpha\to\beta} = \exp\left(\frac{-\Delta v \, b_{\alpha\to\beta}}{k\,\theta}\right) \quad , \tag{33}$$

with k being Boltzmann's constant, Δv denoting the (constant) transformation region's volume, θ representing the current temperature and $b_{\alpha\to\beta}$ being the energy barrier for the transformation under consideration, i.e. from phase α to phase β. Note that $b_{\alpha\to\beta} \neq b_{\beta\to\alpha}$ and thus $P_{\alpha\to\beta} \neq P_{\beta\to\alpha}$ holds in general. The energy barriers follow from the evaluation of certain Gibbs energy states as elaborated in detail in Section 2.7.

2.7 COMPUTATION OF GIBBS ENERGY BARRIERS

For the computation of Gibbs energy barriers that need to be overcome for the transformation from one phase into another, the minima of the individual Gibbs energy functions $\widehat{g}^{\alpha}_N(\lambda^*_N)$ specified in (22) as well as the Gibbs energy value at the intersection point of the two involved potentials need to be determined. To this end, in the context of the considered two-phase setup, we determine the minima of the austenite and martensite Gibbs free energies in the λ^*_N parameter space via

$$\lambda^{\mathrm{A}}_{\min} = \arg\min \widehat{g}^{\mathrm{A}}_N(\lambda^*_N) \tag{34}$$

and

$$\lambda^{\mathrm{M}}_{\min} = \arg\min \widehat{g}^{\mathrm{M}}_N(\lambda^*_N) \; , \tag{35}$$

respectively. The associated minimal Gibbs free energy values for both phases are then evaluated as

$$g^{\mathrm{A}}_{\min} = \widehat{g}^{\mathrm{A}}_N(\lambda^{\mathrm{A}}_{\min}) \tag{36}$$

and

$$g^{\mathrm{M}}_{\min} = \widehat{g}^{\mathrm{M}}_N(\lambda^{\mathrm{M}}_{\min}) \; . \tag{37}$$

Moreover, the intersection point of both potentials in the fictitious strain space parameterised by λ^*_N yields

$$\widehat{g}^{\mathrm{A}}_N(\lambda^*_N) = \widehat{g}^{\mathrm{M}}_N(\lambda^*_N) \tag{38}$$

$$\Rightarrow \quad \widehat{g}^{\mathrm{A}}_N(\lambda^*_N) - \widehat{g}^{\mathrm{M}}_N(\lambda^*_N) = 0 \; , \tag{39}$$

which is solved using a minimisation procedure in terms of

$$\lambda^{\mathrm{isc}}_{\min} = \arg\min | \, \widehat{g}^{\mathrm{A}}_N(\lambda^*_N) - \widehat{g}^{\mathrm{M}}_N(\lambda^*_N) \, | \; , \tag{40}$$

where the superscript 'isc' stands for 'intersection'. The obtained solution $\lambda^{\mathrm{isc}}_{\min}$ therefore corresponds to the specific point in the fictitious strain space at which the Gibbs energy potentials of both phases take the same value, i.e.

$$\widehat{g}^{\mathrm{A}}_N(\lambda^{\mathrm{isc}}_{\min}) = \widehat{g}^{\mathrm{M}}_N(\lambda^{\mathrm{isc}}_{\min}) \; . \tag{41}$$

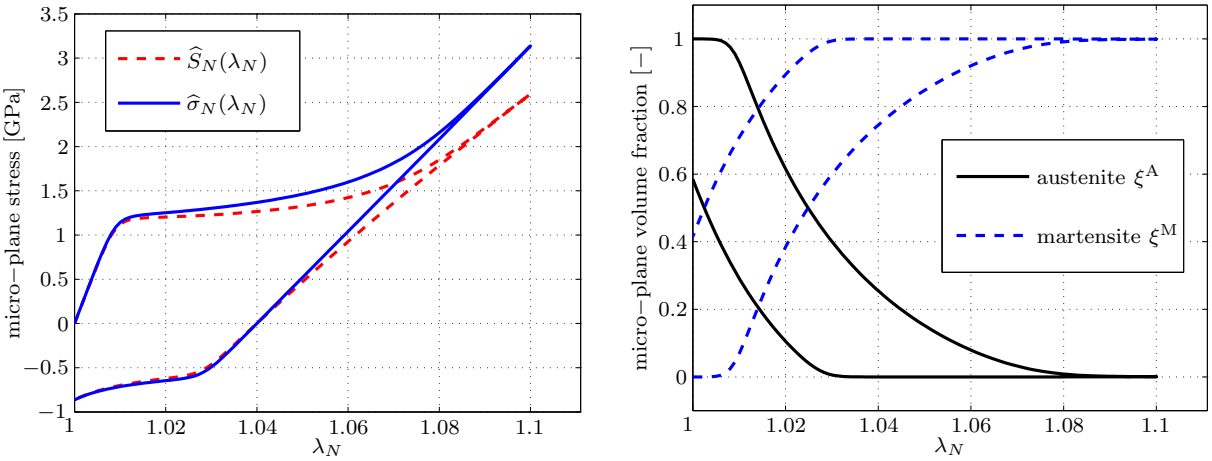

(a) Stress-stretch response.

(b) Micro-plane evolution of volume fractions.

Figure 1: Micro-plane results: evolution of stress and volume fractions due to an artificially prescribed time-proportional ramp-type micro-plane normal stretch $\lambda_N(t)$ up to a maximum stretch of $\lambda_N(t = 1\,\mathrm{s}) = 1.1$. The load is then reversed to a state of zero stretch, $\lambda_N(t = 2\,\mathrm{s}) = \lambda_N(t = 0) = 1$.

The Gibbs energy barrier $b_{\mathrm{A}\to\mathrm{M}}$ for the transformation from austenite A to martensite M then follows from

$$b_{\mathrm{A}\to\mathrm{M}} = \widehat{g}^{\mathrm{A}}_N(\lambda^{\mathrm{isc}}_{\mathrm{min}}) - g^{\mathrm{A}}_{\mathrm{min}} \,, \tag{42}$$

whereas the Gibbs energy barrier $b_{\mathrm{M}\to\mathrm{A}}$ for the reverse transformation, i.e. from martensite M to austenite A, follows in a similar way according to

$$b_{\mathrm{M}\to\mathrm{A}} = \widehat{g}^{\mathrm{M}}_N(\lambda^{\mathrm{isc}}_{\mathrm{min}}) - g^{\mathrm{M}}_{\mathrm{min}} \,. \tag{43}$$

With the aforementioned quantities at hand, the system of evolution equations (29) is fully specified and can thus be solved with the help of standard numerical time-integration schemes.

2.8 NUMERICAL EXAMPLE ON THE MICRO-PLANE LEVEL

For the numerical example on the micro-plane level, we consider a stretch-driven deformation and evaluate the stress response (17) as well as the deformation-driven evolution of internal variables, i.e. volume fractions ξ^{A} and ξ^{M}, cf. (29). Given the two-phase setup considered in the contribution at hand, for the transformation strain of the austenitic parent phase A we set $\lambda^{\mathrm{A}}_{\mathrm{tr}} = 1$ and for the martensite phase M we choose $\lambda^{\mathrm{M}}_{\mathrm{tr}} = 1.04$. Further parameters are chosen as $\omega = 16\,\mathrm{s}^{-1}$, $\Delta v = 2.71 \times 10^{-8}\,\mathrm{mm}^3$, and $\theta = 273\,\mathrm{K}$, see Section 2.6.

The numerical results obtained for a prescribed micro-plane stretch λ_N with time-proportional quasi-static loading are depicted in Fig. 1. The stress-stretch relation shows a plateau-type stress evolution within the material as soon as the martensite transformation is activated at approximately $\lambda_N \approx 1.01$. At this deformation state, the austenitic parent phase starts to decrease, while at the same time the martensite volume fraction increases, cf. Fig. 1(b). As the martensitic transformation is completed, i.e. at $\xi^{\mathrm{M}} \to 1$ as $\lambda_N \to 1.08$, further stretch of the material induces a linear increase in elastic martensite stress, cf. Fig. 1(a). In addition to the micro-plane material stress measure $S_N = \widehat{S}_N(\lambda_N)$, cf. (17), we compute the micro-plane Cauchy stress $\sigma_N = \widehat{\sigma}_N(\lambda_N)$ via $\widehat{\sigma}_N(\lambda_N) = \lambda_N^4\, \widehat{S}_N(\lambda_N)/J^2$, see [33], where $J = \det(\boldsymbol{F})$ denotes the determinant of the macroscopic deformation gradient $\boldsymbol{F}$. In the context of the artificially applied micro-plane strain, however, we choose $J = \lambda_N$.

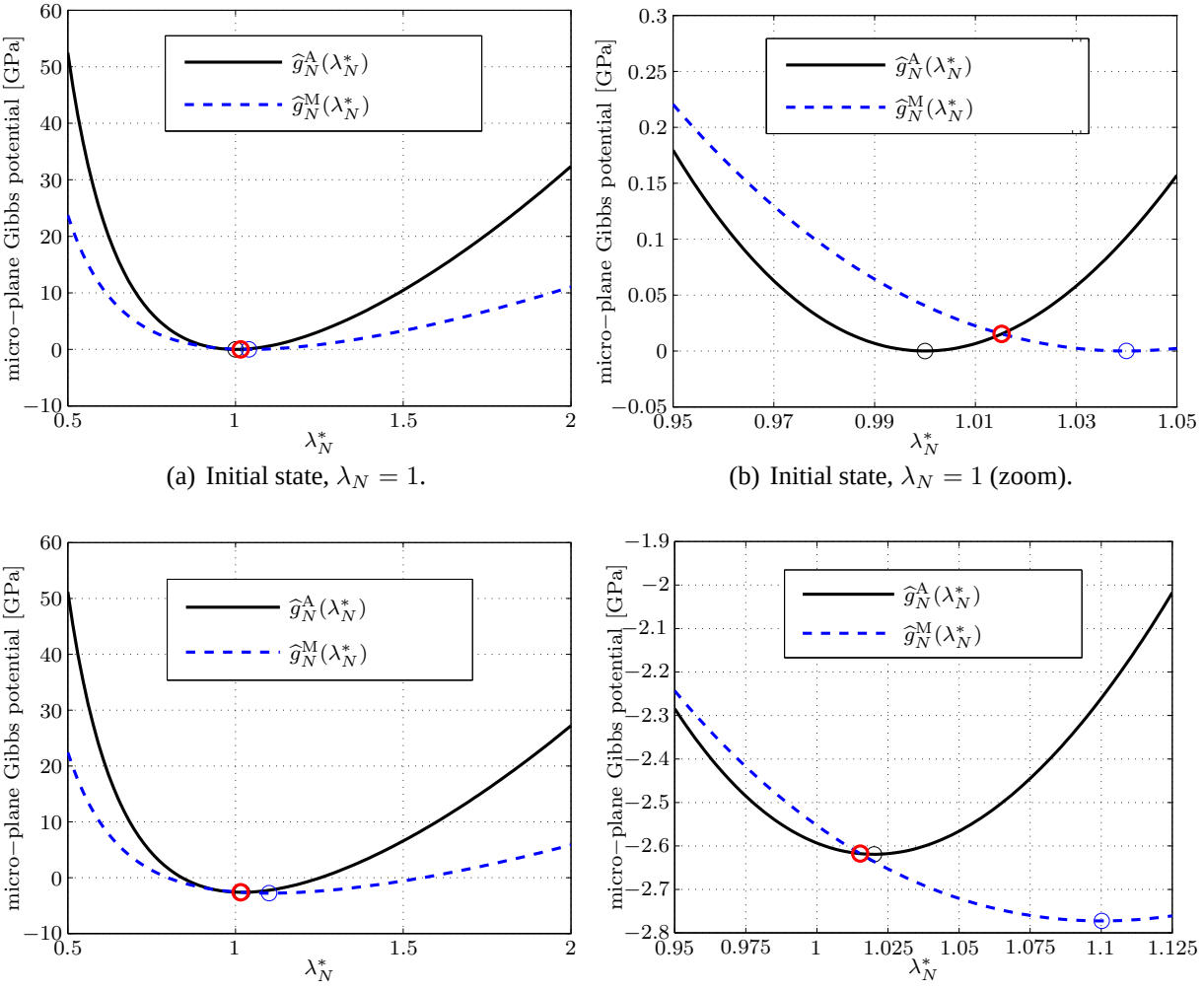

(a) Initial state, $\lambda_N = 1$.

(b) Initial state, $\lambda_N = 1$ (zoom).

(c) Stretched state, $\lambda_N = 1.1$.

(d) Stretched state, $\lambda_N = 1.1$ (zoom).

Figure 2: Micro-plane Gibbs potentials for austenite and martensite, g_N^{A} and g_N^{M}, respectively, at two selected material stretch states λ_N. Note that $\lambda_N = 1$ refers to the initial, undeformed configuration and that λ_N^* is a fictitious stretch used for parameterisation of g_N, cf. Section 2.5.

The Gibbs energy potentials of the individual phases as derived in (22) are provided in Fig. 2 for both the initial material state and the state of maximum stretch, i.e. for states of $\lambda_N(t = 0) = 0$ and $\lambda_N(t = 1\,\mathrm{s}) = 1.1$, respectively. The non-quadratic nature of both micro-plane Gibbs energy potentials—as resulting from the specific form of the underlying Helmholtz free energy definition (6)—is shown in Figs. 2(a) and 2(c).

A closer look at the intersection points of the individual phase potentials—cf. Figs. 2(b) and 2(d)—reveals the location of the Gibbs energy minima in relation to the Gibbs energy value at the intersection point. The minimum-related Gibbs energy values, (36) and (37), as well as the Gibbs energy value at the intersection point (41) need to be computed in order to obtain the Gibbs energy barriers, (42) and (43), which define the transformation probabilites (33) and thus drive the evolution of volume fractions (29).

3 MICRO-SPHERE APPLICATION

Following [33], the macroscopic Piola-Kirchhoff stress tensor $\boldsymbol{S}$ is computed based on the individual material micro-plane stress measures $\widehat{S}(\lambda_N)$ via integration over the unit hemisphere

in terms of

$$\boldsymbol{S} = \frac{3}{2\,\pi} \int_{\mathbb{H}^2} \widehat{S}(\lambda_N)\, \lambda_N^{-1}\, \boldsymbol{N} \otimes \boldsymbol{N}\, \mathrm{d}\omega \,. \tag{44}$$

For the macroscopic Cauchy stress response $\boldsymbol{\sigma}$ depicted in Fig. 3, we apply the standard push-forward of $\boldsymbol{S}$ viz.

$$\boldsymbol{\sigma} = \frac{1}{J}\, \boldsymbol{F} \cdot \boldsymbol{S} \cdot \boldsymbol{F}^{\mathrm{t}} \,. \tag{45}$$

The quasi-static application of a macroscopic non-isochoric homogeneous state of tensile deformation

$$\boldsymbol{F}(t) = \boldsymbol{I} + \kappa(t)\, \boldsymbol{e}_1 \otimes \boldsymbol{e}_1 \tag{46}$$

with $\kappa(t) \in [0, 0.2] \subset \mathbb{R}$ introduced as a time-proportional load scaling parameter results in the macroscopic material response provided in Fig. 3. The obtained Cauchy stress response, Fig. 3(a), shows a plateau-type stress characteristic that is related to the deformation-induced onset of martensitic transformation within the polycrystal. The macroscopic volume fractions $\Xi^{\bullet}$—homogenised in terms of a moment of zeroth order—show a saturation-type evolution, i.e. even for very large deformations the polycrystal will not transform to 100% martensite.

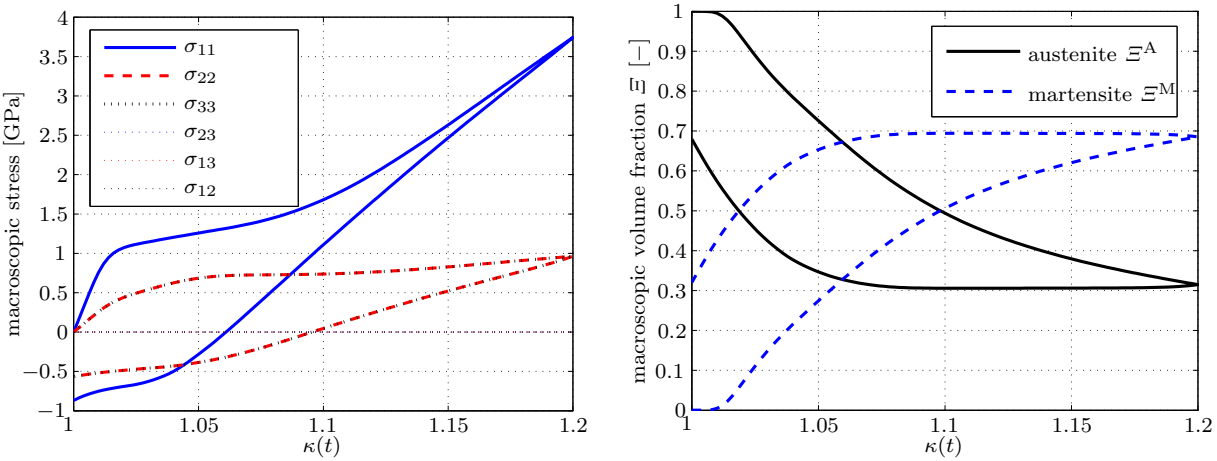

(a) Macroscopic Cauchy stress evolution.

(b) Macroscopic volume fractions.

Figure 3: Application of the micro-sphere framework: evolution of stress and volume fractions due to a quasi-statically applied macroscopic non-isochoric homogeneous state of tensile deformation in terms of $\boldsymbol{F}(t) = \boldsymbol{I} + \kappa(t)\, \boldsymbol{e}_1 \otimes \boldsymbol{e}_1$.

4 CONCLUSIONS

The contribution at hand introduces a constitutive formulation that extends an established finite strain micro-sphere framework for the simulation of Neo-Hookean-type materials towards phase-transformations between austenite and martensite. Individual micro-plane free energy terms are assigned to both phases, where the Helmholtz free energy of martensite is consistently extended to include a Bain-type transformation strain which is multiplicatively coupled to the overall micro-plane strain measure of the martensite fraction.

The numerical examples obtained at both the micro-plane level, see Section 2.8, and at the micro-sphere level, see Section 3, show that the proposed modelling framework—even though not yet fitted to experimental data—is able to capture the typical, experimentally observed stress-strain behaviour of, e.g., shape memory alloys. Moreover, the proposed micro-sphere

formulation naturally captures the polycrystalline transformation behaviour that is related to the so-called grain-locking effect as introduced in Section 1.

In conclusion, the proposed micro-sphere based finite strain modelling framework for phase-transformations can be considered as a promising foundation in view of later extensions towards coupled plasticity and temperature effects in polycrystals.

REFERENCES

[1] S. Miyazaki, "Medical and dental applications of shape memory alloys," *Shape Memory Materials, Cambridge University Press*, vol. 12, pp. 267–281, 1999.

[2] D. Hartl and D. Lagoudas, "Aerospace applications of shape memory alloys," *P. I. Mech. Eng. G: J. Aer.*, vol. 221, pp. 535–552, 2007.

[3] K. Otsuka and T. Kakeshita, "Science and technology of shape-memory alloys: new developments," *MRS Bull*, vol. 27, pp. 91–100, 2002.

[4] T. Merzouki, A. Duval, and T. B. Zineb, "Finite element analysis of a shape memory alloy actuator for a micropump," *Sim. Mod. Pract. Theory*, vol. 27, pp. 112–126, 2012.

[5] L. Brinson, I. Schmidt, and R. Lammering, "Stress-induced transformation behavior of a polycrystalline NiTi shape memory alloy: micro and macromechanical investigations via in situ optical microscopy," *J. Mech. Phys. Solids*, vol. 52, no. 7, pp. 1549–1571, 2004.

[6] S. Govindjee, A. Mielke, and G. Hall, "The free energy of mixing for n-variant martensitic phase transformations using quasi-convex analysis," *J. Mech. Phys. Solids*, vol. 50, pp. 1897–1922, 2002.

[7] T. Bartel and K. Hackl, "A micromechanical model for martensitic phase-transformations in shape-memory alloys based on energy-relaxation," *J. Appl. Math. Mech.*, vol. 89 (10), pp. 792–809, 2009.

[8] K. Hackl and R. Heinen, "An upper bound to the free energy of n-variant polycrystalline shape memory alloys," *J. Mech. Phys. Solids*, vol. 56, pp. 2832–2843, 2008.

[9] C. Collard and T. B. Zineb, "Simulation of the effect of elastic precipitates in SMA materials based on a micromechanical model," *Comp. Part B: Eng.*, vol. 43, no. 6, pp. 2560–2576, 2012.

[10] A. S. J. Suiker and S. Turteltaub, "Numerical modelling of transformation-induced damage and plasticity in metals," *Model. Simul. Mater. Sc.*, vol. 15, pp. 147–166, 2007.

[11] S. Turteltaub and A. S. J. Suiker, "Grain size effects in multiphase steels assisted by transformation-induced plasticity," *Int. J. Sol. Struct.*, vol. 43, no. 24, pp. 7322–7336, 2006.

[12] A. S. J. Suiker and B. Thijsse, "Nucleation, kinetics and morphology of displacive phase transformations in iron," *J. Mech. Phys. Solids*, vol. 61, no. 11, pp. 2273–2301, 2013.

[13] T. Bartel, B. Kiefer, K. Buckmann, and A. Menzel, "A kinematically-enhanced relaxation scheme for the modeling of displacive phase transformations," *J. Intel. Mat. Syst. Str.*, vol. 26, no. 6, pp. 701–717, 2015.

[14] T. Bartel and A. Menzel, "Partially relaxed energy potentials for the modelling of microstructures – application to shape memory alloys," *GAMM-Mitteilungen*, vol. 35, no. 1, pp. 59–74, 2012.

[15] D. Helm and P. Haupt, "Shape memory behaviour: modelling within continuum mechanics," *Int. J. Sol. Struct.*, vol. 40, pp. 827–849, 2003.

[16] F. Auricchio and R. Taylor, "Shape-memory alloys: modelling and numerical simulations of the finite-strain superelastic behavior," *Comput. Method. Appl. M.*, vol. 143, pp. 175–194, 1997.

[17] B. Raniecki, C. Lexcellent, and K. Tanaka, "Thermodynamic models of pseudoelastic behaviour of shape memory alloys," *Arch. Mech.*, vol. 44, pp. 261–284, 1992.

[18] C. Truesdell and R. Toupin, "The classical field theories," in *Handbuch der Physik* (S. Flügge, ed.), vol. 3, Berlin: Springer, 1960.

[19] D. Hartl and D. Lagoudas, "Constitutive modeling and structural analysis considering simultaneous phase transformations and plastic yield in shape memory alloys," *Smart Mater. Struct.*, vol. 18, no. 10, pp. 1–17, 2009.

[20] D. Helm, *Formgedächtnislegierungen – Experimentelle Untersuchung, phänomenologische Modellierung und numerische Simulation der thermomechanischen Materialeigenschaften*. Dissertation, Universität Gesamthochschule Kassel, 2001. Berichte des Instituts für Mechanik (Bericht 3/2001).

[21] D. Helm and P. Haupt, "Thermomechanical behaviour of shape memory alloys," *Proceedings of SPIEs Smart Structures and Materials*, vol. 4333, pp. 302–313, 2001.

[22] K. Tanaka, "A thermomechanical sketch of shape memory effect: one-dimensional tensile behavior," *Res. Mech*, vol. 18, pp. 251–263, 1986.

[23] S. Reese and D. Christ, "Finite deformation pseudo-elasticity of shape memory alloys – constitutive modelling and finite element implementation," *Int. J. Plasticity*, vol. 24, pp. 455–482, 2008.

[24] S. Govindjee and C. Miehe, "A multi-variant martensitic phase transformation model: formulation and numerical implementation," *Comput. Method. Appl. M.*, vol. 191, no. 3-5, pp. 215–238, 2001.

[25] E. Stein and O. Zwickert, "Theory and finite element computations of a unified cyclic phase transformation model for monocrystalline materials at small strains," *Comput. Mech.*, vol. 40, no. 3, pp. 429–445, 2007.

[26] E. Patoor, D. Lagoudas, P. Entchev, L. Brinson, and X. Gao, "Shape memory alloys, part I: general properties and modeling of singlecrystals," *Mech. Mater.*, vol. 38, pp. 391–429, 2006.

[27] M. Achenbach, "A model for an alloy with shape memory," *Int. J. Plasticity*, vol. 5, pp. 371–395, 1989.

[28] S. Govindjee and G. Hall, “A computational model for shape memory alloys,” *Int. J. Sol. Struct.*, vol. 37, pp. 735–760, 2000.

[29] R. Ostwald, T. Bartel, and A. Menzel, “A computational micro-sphere model applied to the simulation of phase-transformations,” *J. Appl. Math. Mech.*, vol. 90, no. 7-8, pp. 605–622, 2010.

[30] R. Ostwald, T. Bartel, and A. Menzel, “Phase-transformations interacting with plasticity – a micro-sphere model applied to TRIP steel,” *Comp. Mater. Sci.*, vol. 64, pp. 12–16, 2012.

[31] R. Ostwald, T. Bartel, and A. Menzel, “A Gibbs-energy-barrier-based computational micro-sphere model for the simulation of martensitic phase-transformations,” *Int. J. Numer. Meth. Eng.*, vol. 97, pp. 851–877, 2014.

[32] R. Ostwald, T. Bartel, and A. Menzel, “An energy-barrier-based computational micro-sphere model for phase-transformations interacting with plasticity,” *Comput. Method. Appl. M.*, vol. 293, pp. 232–265, 2015.

[33] I. Carol, M. Jirásek, and Z. Bažant, “A framework for microplane models at large strain, with application to hyperelasticity,” *Int. J. Sol. Struct.*, vol. 41, pp. 511–557, 2004.